

# Inflammation-Induced Hepatocellular Carcinoma Is Dependent on CCR5 in Mice

Neta Barashi,<sup>1</sup> Ido D. Weiss,<sup>1</sup> Ori Wald,<sup>1</sup> Hanna Wald,<sup>1</sup> Katia Beider,<sup>1</sup> Michal Abraham,<sup>1</sup> Shiri Klein,<sup>1</sup> Daniel Goldenberg,<sup>1</sup> Jonathan Axelrod,<sup>1</sup> Eli Pikarsky,<sup>2</sup> Rinat Abramovitch,<sup>1,3</sup> Evelyne Zeira,<sup>1</sup> Ethan Galun,<sup>1</sup> and Amnon Peled<sup>1</sup>

**H**uman hepatocellular carcinoma (HCC) is an inflammation-induced cancer, which is the third-leading cause of cancer mortality worldwide. We investigated the role of the chemokine receptors, CCR5 and CCR1, in regulating inflammation and tumorigenesis in an inflammation-induced HCC model in mice. Multidrug resistance 2 gene (Mdr2)-knockout (Mdr2-KO) mice spontaneously develop chronic cholestatic hepatitis and fibrosis that is eventually followed by HCC. We generated two new strains from the Mdr2-KO mouse, the Mdr2:CCR5 and the Mdr2:CCR1 double knockouts (DKOs), and set out to compare inflammation and tumorigenesis among these strains. We found that in Mdr2-KO mice lacking the chemokine receptor, CCR5 (Mdr2:CCR5 DKO mice), but not CCR1 (Mdr2:CCR1 DKO), macrophage recruitment and trafficking to the liver was significantly reduced. Furthermore, in the absence of CCR5, reduced inflammation was also associated with reduced periductal accumulation of CD24<sup>+</sup> oval cells and abrogation of fibrosis. DKO mice for Mdr2 and CCR5 exhibited a significant decrease in tumor incidence and size. **Conclusions:** Our results indicate that CCR5 has a critical role in both the development and progression of liver cancer. Therefore, we propose that a CCR5 antagonist can serve for HCC cancer prevention and treatment. (HEPATOLOGY 2013;58:1021-1030)

**I**n 1863, Virchow hypothesized that cancer originated at sites of chronic inflammation. Indeed, a growing body of evidence indicates that many malignancies are initiated by infections and chronic inflammation, accounting for over 20% of malignancy cases worldwide. However, the molecular and cellular mechanisms revealing how chronic inflammation leads to tumorigenesis remain largely unknown.<sup>1-3</sup> Human hepatocellular carcinoma (HCC), a primary malignancy of the liver and the third-leading cause of cancer

mortality worldwide,<sup>4,5</sup> is an example of inflammation-induced cancer. In humans, chronic viral hepatitis, metabolic liver diseases, and alcohol abuse cause chronic inflammation; this, in turn, can induce fibrosis, cirrhosis, and cancer.<sup>6,7</sup> Chemokines and chemokine receptors function in the initiation and maintenance of inflammation and fibrosis<sup>1</sup> and might play a crucial role in the chronic inflammation that leads to tumorigenesis.<sup>8,9</sup> CCR1 and CCR5, members of the G-protein-coupled receptor superfamily, are functional receptors for several

**Abbreviations:** Ab, antibody;  $\alpha$ -SMA, alpha smooth muscle actin; ALT, alanine aminotransferase; AST, aspartate aminotransferase; BM, bone marrow; BrdU, bromodeoxyuridine; cDNA, complementary DNA; CFSE, carboxyfluorescein diacetate succinimidyl ester; CK, cytokeratin; DKO, double knockout; ELISA, enzyme-linked immunosorbent assay; EpCAM, epithelial cell adhesion molecule; FACS, fluorescence-activated cell sorting; FCS, fetal calf serum; HCC, hepatocellular carcinoma; H&E, hematoxylin and eosin; HSCs, hepatic stellate cells; Igfbp, insulin-like growth factor-binding protein; IHC, immunohistochemical; IL, interleukin; IP, intraperitoneally; KO, knockout; krt19, keratin 19; Mdr2, multidrug resistance 2 gene; MIP-1 $\alpha/\beta$ , macrophage inflammatory protein 1 alpha/beta; M-MLV, Moloney murine leukemia virus; MMPs, matrix metalloproteinases; MRI, magnetic resonance imaging; mRNA, messenger RNA; PBMCs, peripheral blood mononuclear cells; PBS, phosphate-buffered saline; PCR, polymerase chain reaction; RANTES, regulated upon activation normal T cell expressed and presumably secreted; RT, reverse transcription; spp1, secreted phosphoprotein 1; TGF- $\beta$ , transforming growth factor beta; TNF- $\alpha$ , tumor necrosis factor alpha; WT, wild type.

From the <sup>1</sup>Goldyne Savad Institute of Gene Therapy; <sup>2</sup>Department of Pathology, Human Biology Research Center, Hadassah Hebrew University Hospital, Jerusalem, Israel.

Received October 27, 2012; accepted March 15, 2013.

Contract grant sponsor: This research was supported by a research fund from the Chief Scientist Office of the Israeli Ministry of Health (grant no.: 300000-6147), the Deutsche Forschungsgemeinschaft (grant no.: SFB871), as well as by a grant from the Israeli Ministry of Health.

inflammatory CC chemokines, including macrophage inflammatory protein 1 (MIP)-1 $\alpha$ , MIP-1 $\beta$ , and regulated upon activation normal T cell expressed and secreted (RANTES), and are expressed on peripheral blood leukocytes, including macrophages, natural killer cells, and T cells.<sup>10,11</sup> In a previous study, we demonstrated that CCR5, but not CCR1, regulates the trafficking of immune cells into the liver under normal conditions.<sup>12</sup> In addition, we also reported that in multidrug resistance 2 gene (Mdr2)-knockout (Mdr2-KO) mice, a strain that spontaneously develops chronic cholestatic hepatitis and fibrosis that is eventually followed by HCC,<sup>13-15</sup> the RANTES chemokine is highly expressed.<sup>16</sup> RANTES is a ligand for both CCR1 and CCR5. Based on these observations, we propose, in this study, that the trafficking of immune cells to the liver mediated by CCR5 is critical for the development of inflammation-induced HCC.<sup>12,17</sup> To test this hypothesis, we studied the role of CCR1 and CCR5 in Mdr2-KO mice. Therefore, we generated two new strains from the Mdr2-KO mouse, the Mdr2:CCR5 and the Mdr2:CCR1 double knockouts (DKOs), and set out to compare inflammation and tumorigenesis among these strains.

## Material and Methods

**Mice.** Animal experiments were performed according to a protocol approved by the animal care committee of Hebrew University (Jerusalem, Israel). All animals were kept on a 12-hour light/dark cycle in a pathogen-free animal facility with free access to food and water. Wild-type (WT) C57Bl/6J and CCR5-deficient mice were purchased from The Jackson Laboratory (Bar Harbor, ME). CCR1-deficient mice were acquired from Taconic Farms (Germantown, NY). FVB.129P2-Abcb4tm1Bor (Mdr2-KO; The Jackson Laboratory) mice were kindly given to us by Dr. Daniel Goldenberg from the Goldyne Savad Institute of Gene Therapy Hadassah University Hospital (Jerusalem, Israel) and crossed into the C57Bl/6 genetic background for at least nine generations. Double-mutant Mdr2:CCR5 and Mdr2:CCR1 DKO mice were generated by crossing Mdr2-KO with either CCR5- or CCR1-deficient mice and their progeny were identified by polymerase chain

reaction (PCR) analysis (for primer sequences, see the Supporting Materials). At ages of 1, 3, and 16 months, mice were sacrificed by a lethal dose of isoflurane anesthesia and livers were excised and weighed. All mice were injected intraperitoneally (IP) with bromodeoxyuridine (BrdU; Sigma-Aldrich, Rehovot, Israel) at 1 mg/mouse in 10  $\mu$ L per 1 g of body weight 3 and 24 hours before sacrifice. Liver specimens were either fixed in 4% buffered formalin or snap-frozen in liquid nitrogen for further analysis.

**Blood Sample Analysis.** Blood samples were collected monthly from the age of 1 month until 6 months by tail vein bleeding. Levels of liver enzymes in sera, including alanine aminotransferase (ALT), aspartate aminotransferase (AST), and alkaline phosphatase, were measured with Reflotron (Roche, Mannheim, Germany).

**Magnetic Resonance Imaging Analysis.** Magnetic resonance imaging (MRI) was performed on a horizontal 4.7T BioSpec spectrometer (Bruker Corporation, Billerica, MA), using a birdcage coil. Mice were anesthetized (30 mg/kg of pentobarbital IP) and placed in a supine position, with the liver located at the center of the coil. Eight mice from each group (i.e., Mdr2-KO, Mdr2:CCR5 DKO, and Mdr2:CCR1 DKO) were scanned at 9, 13, and 16 months, and liver hepatomegaly and tumor formation were evaluated from multi-slice coronal and axial T1- and T2-weighted fast-spin echo images covering the entire liver, both coronally and axially (repetition time/echo time = 147/10 ms; flip angle = 30 degrees; field of view = 5 cm; 256  $\times$  256 pixels; 11-13 slices with slice thickness = 1 mm).

**Transwell Migration Assays.** Mouse peripheral blood mononuclear cells (PBMCs) were analyzed for the ability to migrate toward RANTES *in vitro*. For this aim, 100  $\mu$ L of chemotaxis buffer (RPMI 1640, 1% fetal calf serum [FCS]; Biological Industries, Kibbutz Beth Haemek, Israel) containing  $2 \times 10^5$  PBMCs from either WT, CCR5-, or CCR1-deficient mice were placed into the upper chamber of a Costar 24-well transwell (Costar, Cambridge, MA), and 600  $\mu$ L of chemotaxis buffer with or without RANTES (PeproTech EC, London, UK) were added to the bottom chamber (at indicated concentration). Cells were collected from

Address reprint requests to: Amnon Peled, Ph.D., Gene Therapy Institute, Hadassah University Hospital, P.O. Box 12000, Jerusalem 91120, Israel. E-mail: peled@hadassah.org.il; fax: +972-2-6430982.

Copyright © 2013 by the American Association for the Study of Liver Diseases.

View this article online at [wileyonlinelibrary.com](http://wileyonlinelibrary.com).

DOI 10.1002/hep.26403

Potential conflict of interest: Nothing to report.

Additional Supporting Information may be found in the online version of this article.

the chambers after 4 hours of migration at 37°C, stained with antimouse Mac-1 (eBioscience, San Diego, CA), and counted by flow cytometry.

**Western Blotting Analysis.** Liver samples were homogenized in homogenization buffer (50 mmol/L of Tris-HCl [pH 7.6], 0.25% Triton X-100, 0.15 M of NaCl, 10 mM of CaCl<sub>2</sub>, and complete mini-ethylene-nediaminetetraacetic acid-free protease inhibitor cocktail [Roche Diagnostics, Mannheim, Germany]). Tissue lysates (containing 30 µg of protein) were separated on a 10% sodium dodecyl sulfate polyacrylamide gel. Blottings were incubated overnight at 4°C in a blocking buffer containing 5% skim milk and then incubated with either anti-SMA (smooth muscle actin) (Dako, Carpinteria, CA) or beta-actin (Sigma-Aldrich) mouse monoclonal antibody (Ab) (diluted 1:2,000) for 2 hours at room temperature and, subsequently, with peroxidase-conjugated goat antimouse immunoglobulin G (Dako) for 1 hour at room temperature.

**RNA Extraction and Real-Time PCR.** Total RNA was extracted from livers of 1- and 3-month-old mice (WT, Mdr2-KO, Mdr2:CCR5 DKO, and Mdr2:CCR1 DKO) using TRIzol reagent (Invitrogen Life Technologies, Carlsbad, CA), according to the protocol recommended by the manufacturer. Complementary DNA (cDNA) was obtained by reverse transcription (RT) of 1 mg of total RNA in a final reaction volume of 25 µL containing 1× Moloney murine leukemia virus (M-MLV) RT buffer, 2.5 µmol/L of random hexamers, 0.5 mmol/L of each deoxynucleoside triphosphate, 3 mmol/L of MgCl<sub>2</sub>, 0.4 U/µL of RNase inhibitor, and 100 U/µL of M-MLV RT (Promega, Madison, WI). Quantitative real-time PCR assays, containing the primers and probe mix for transforming growth factor beta (TGF-β) and RANTES, were purchased from Applied Biosystems (Foster City, CA) and utilized according to the manufacturer's instructions. PCR reactions were carried out in a final reaction volume of 20 µL containing 100 ng of cDNA template, 10 µL of TaqMan Universal Master Mix (Applied Biosystems), and 1 µL of gene and probe mix. All reactions were run in triplicate, and the housekeeping gene, glyceraldehyde 3-phosphate dehydrogenase (Applied Biosystems), was amplified in a parallel reaction for normalization.

**In Vivo Distribution Analysis of Carboxyfluorescein Diacetate Succinimidyl Ester–Labeled Cells.** Bone marrow (BM) cells were isolated from the tibia and femur of either WT, CCR5 KO, or CCR1 KO mice, filtered through a cell strainer fluorescence-activated cell sorting (FACS) tube (Falcon; BD Biosciences, San Jose, CA), washed twice in sterile phosphate-buffered saline

(PBS), and diluted to 5 × 10<sup>7</sup> cells/mL. Purified BM cells were labeled with 0.5 µg/mL of carboxyfluorescein diacetate succinimidyl ester (CFSE) (BCECF/AM; Calbiochem, Nottingham, UK) for 15 minutes, washed in PBS, and treated with FCS to neutralize CFSE activity. Labeled BM cells were injected into the tail vein of 3-month-old Mdr2-KO or WT mice (2 × 10<sup>6</sup> cells per mouse in a total volume of 200 µL). After 48 hours, mice were sacrificed and livers were harvested. Liver tissue was homogenized and immune cells were collected on a Ficoll gradient (Histopaque-1077-1; Sigma-Aldrich). Recruitment of total CFSE-positive cells and CFSE-F4/80 (Alexa Fluor 647 antimouse F4/80; eBioscience) double-positive cells to the liver were assessed by FACScalibur (Becton Dickinson Immunocytometry Systems, San Jose, CA).

**Immunohistochemistry.** For histological analysis, liver tissue was cut into 5-mm sections, deparaffinized with xylene, and hydrated through graded ethanol. Endogenous peroxidase was blocked by incubation for 5 minutes in 3% H<sub>2</sub>O<sub>2</sub>. For γH2AX (05-636; Nippon Biostest Laboratories Inc., Tokyo, Japan), BrdU (M0744; Dako), and nitro tyrosine (AB7048; Abcam, Cambridge, MA) staining, a 25-mM citrate buffer (pH 6.0) was used for antigen retrieval, cooked in a pressure cooker for 20 minutes, and left to cool for 30 minutes at room temperature. Slides were washed in Optimax (Pharmatrade, Dubai, UAE) and incubated with primary Ab (diluted in CAS-Block [Zymed Laboratories, San Francisco, CA] at 1:100, 1:200, and 1:250, respectively) overnight at 4°C. For F4/80 (MCA497; Serotec, Raleigh, NC) and pan-CK (cytokeratin) (Z0622; Dako) staining, antigen retrieval was established by a 5-minute treatment with pronase (Sigma-Aldrich) and 3-hour incubation with the primary Ab (diluted in CAS-Block [Zymed Laboratories] 1:200 and 1:400, respectively) at room temperature. For all staining, we used a conjugated horseradish peroxidase secondary Ab (antimouse and -rabbit [Envision; Dako] and antirat [Histifine; Nichirei, Osaka, Japan]) for 30 minutes and developed it with diaminobenzidine for 5 minutes. Sirius Red staining was performed by incubating deparaffinized and hydrated slides in a 0.1% Sirius Red in picric acid solution for 30 minutes. For the quantitative assessment of F4/80 staining, we used the Ariol system (Genetix USA Inc., San Jose, CA) for automated cell image capture and analysis.

**Enzyme-Linked Immunosorbent Assay.** Serum and liver protein lysate were diluted (1:2) in Calibrator Diluent (from an MMR00 kit), and chemokine levels were determined by enzyme-linked immunosorbent assay (ELISA) using a mouse-RANTES kit (kit

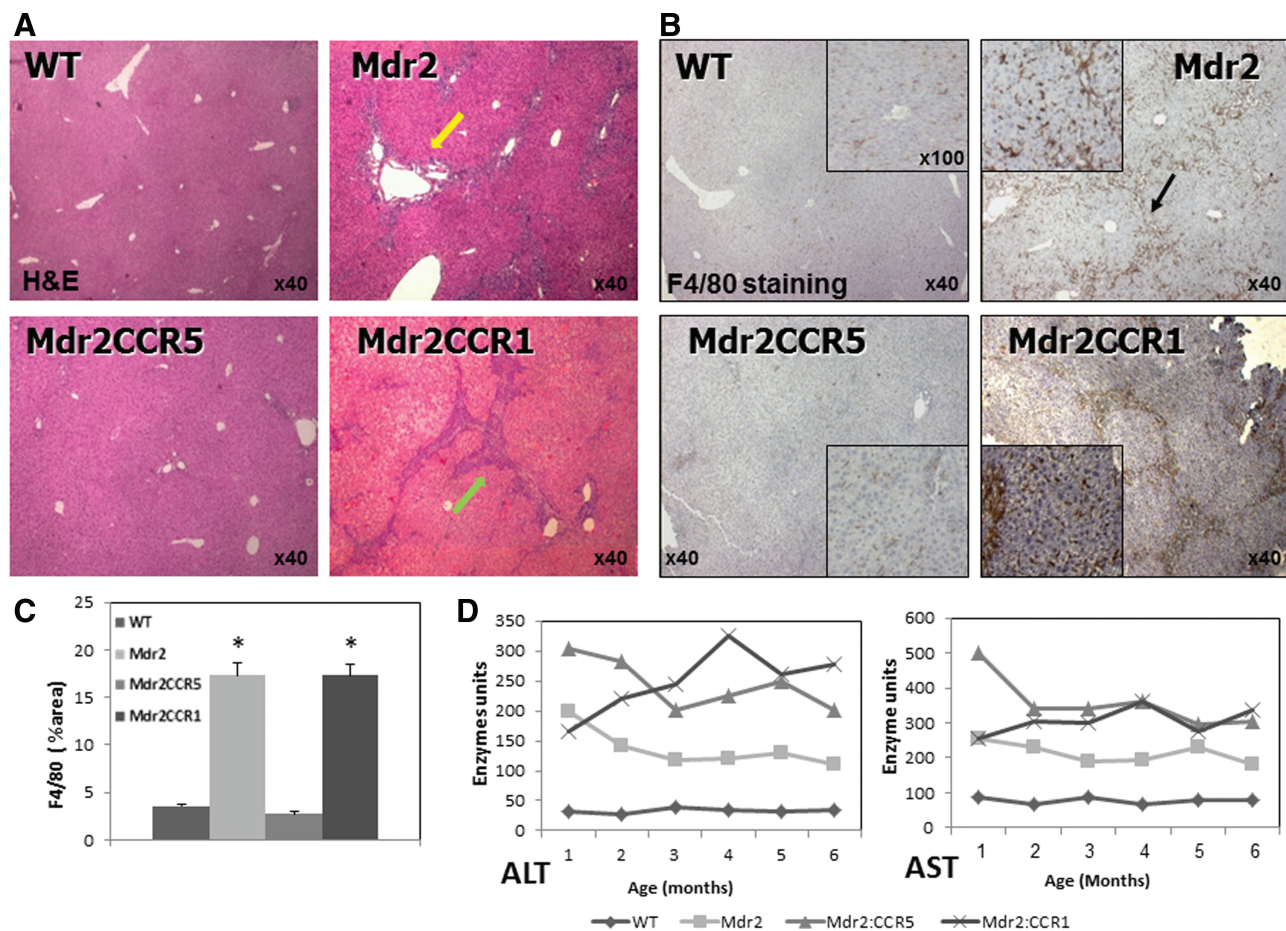


Fig. 1. Liver inflammation and damage is attenuated in the absence of CCR5. (A) H&E-stained sections revealing disturbed periductal architecture (yellow arrow) and infiltration of immune cells to the liver (green arrow) ( $n = 8$ ). (B and C) F4/80 IHC staining for macrophages in 3-month-old WT, Mdr2-KO, Mdr2:CCR5, and Mdr2:CCR1 DKO mice quantified by the Ariol Slide Imaging System (an automated computerized slide imaging information collector) and analyzed by software ( $n = 8$ ; \* $P < 0.01$ ). (D) Liver damage was assessed by measurement of liver enzyme level in serum of 1-month-old to 6-month-old WT, Mdr2-KO, Mdr2:CCR5, and Mdr2:CCR1 DKO mice. All three groups of KO and DKO mice had higher ALT and AST levels, compared to WT controls, indicative of hepatocyte damage ( $n = 15-30$ ).

MMR00; R&D Systems, Minneapolis, MN), according to the manufacturer's specifications.

**Gene Expression.** Preprocessing of the microarray data was done using robust multiarray analysis. Probe-set intensities were transformed to logarithmic scale, and a cutoff of 5 was applied. Probe sets were considered to be differentially expressed if they showed a fold change equal to or greater than 2. This study was supported through the Israeli National Strategic Center For Gene Therapy located in the Goldyne Savad Institute of Gene Therapy at Hadassah University Hospital.

## Results

**Liver Inflammation Is Dependent On CCR5.** In an effort to determine the effect of CCR5 on liver inflammation, we generated the two strains, Mdr2:CCR5 and the Mdr2:CCR1 DKOs. The rational to generate the Mdr2:CCR1 DKO was a result of the fact

that it shares some of the ligands of CCR5 (e.g., RANTES and MIP-1 $\alpha$ ) and therefore would indicate whether the effects we observed were CCR5 specific. Analysis of liver sections revealed that there is a significant difference in inflammation between the Mdr2-KO mouse, the Mdr2:CCR5 DKO, and the Mdr2:CCR1 DKO. Whereas Mdr2-KO and Mdr2:CCR1 DKO mice exhibit massive infiltration of immune cells to the liver, Mdr2:CCR5 DKO mice display significantly reduced inflammation (Fig. 1A). Immunohistochemical (IHC) staining of liver sections revealed a robust accumulation of F4/80 $^{+}$  macrophages and neutrophils in damaged livers of Mdr2-KO and Mdr2:CCR1-DKO mice, but not in Mdr2:CCR5-DKO mice (Fig. 1B,C and Supporting Fig. 1A,B). Overall, Mdr2:CCR5-DKO mice exhibit a significantly less-damaged liver.

Hepatocyte damage was evaluated by measurement of serum ALT and AST. Liver enzyme levels of 1- to 6-month-old mice were measured to assess liver

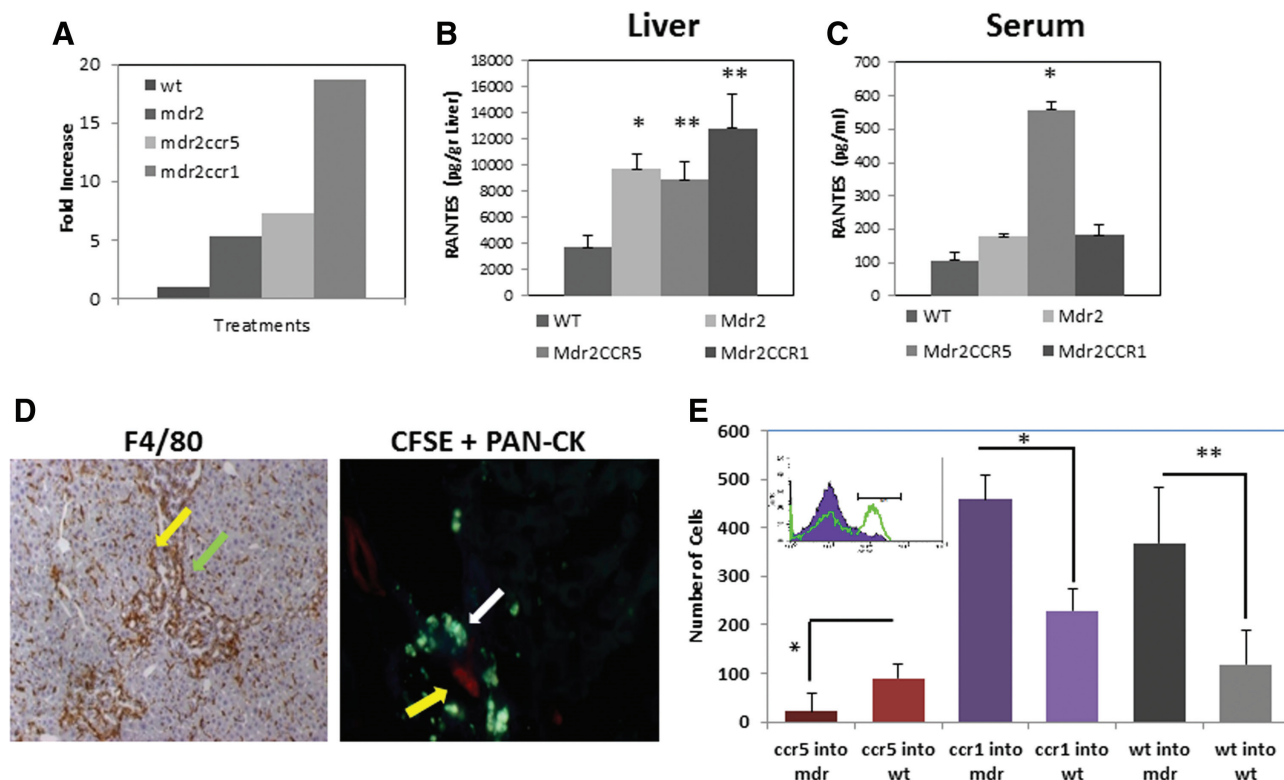


Fig. 2. CCR5 is critical for macrophage recruitment to the liver. (A) Liver expression of RANTES was determined by real-time PCR of liver samples from 3-month-old mice. Figures represented as fold increase, wt = 1 ( $n = 4$ ). (B and C) RANTES levels in the liver (B) and serum (C) of 3-month-old mice determined by ELISA assay ( $n = 3$ ). (D) WT and Mdr2-KO mice were injected with  $2 \times 10^6$  CFSE-labeled cells derived from BM of either WT, CCR5, or CCR1 KO mice. Forty eight hours after injection, mice were sacrificed and livers were harvested for further evaluation of cell recruitment. FACS analysis was used to determine recruitment of CFSE+*F4/80*+ macrophages in livers of WT and Mdr2-KO mice ( $n = 8$ ). (E) Macrophages localize to specific bile duct sites in the liver. High magnification of *F4/80* immunostaining (yellow arrow: bile ducts; green arrow: macrophages) and CFSE-positive recruited cells specifically surround bile duct cells (white arrow: CFSE-positive cells recruited to the liver; yellow arrow: pan-CK staining for bile ducts). For all experiments: \* $P < 0.01$ ; \*\* $P < 0.05$ .

damage. High levels of ALT and AST were detected in the serum of Mdr2-KO, Mdr2:CCR5, and Mdr2:CCR1 DKO mice, compared to WT controls, implying that hepatocyte damage in all three mouse strains was significant, but, in the absence of CCR5, was not accompanied by inflammation (Fig. 1D).

**Inflammatory Reaction in the Portal Triads in the Mdr2-KO Mice Is Dependent on CCR5.** In an effort to understand the molecular, and possibly cellular, mechanism of HCC in Mdr2-KO mice, we performed, in a previous investigation, a gene expression profiling study. This investigation revealed a marked elevation of the inflammatory chemokine, RANTES, a ligand of both CCR1 and CCR5, in the liver of Mdr2-KO FVB.129 mice.<sup>16</sup> Using real-time PCR and ELISA assay, we confirmed that RANTES expression is indeed up-regulated in livers of Mdr2-KO C57Bl6 mice, compared to control C57Bl6 WT mice (Fig. 2A,B). The elevated levels in the liver of RANTES were found in all three strains, compared to WT

mice (Fig. 2B). Surprisingly, we found that the levels of RANTES were increased significantly only in the blood of Mdr2:CCR5 DKO, compared to Mdr2-KO, and Mdr2:CCR1 DKO (Fig. 2C).

Using semiquantitative PCR, we found that in addition to RANTES, the messenger RNA (mRNA) levels of the chemokine, MIP-1 $\alpha$ , which binds both CCR1 and CCR5, was also up-regulated in livers of Mdr2-KO C57Bl6 mice, compared to control C57Bl6 WT and Mdr2:CCR5 DKO mice. In contrast, mRNA levels of MIP-1 $\beta$ , which binds to CCR5, and levels of the homeostatic chemokine, stromal cell-derived factor 1, were only slightly changed (Supporting Fig. 1C).

We hypothesized that the absence of CCR5 is responsible for macrophages' failures to recruit to the damaged liver. To test this hypothesis, CFSE-labeled immune cells derived from WT, CCR1 KO, and CCR5 KO BM were adoptively transferred into both healthy WT and Mdr2-KO recipients. Forty-eight hours after transplantation, recipient WT mice

displayed low levels of macrophage recruitment to the liver, independent of donor cell origin. In contrast, recipient Mdr2-KO mice showed increased liver recruitment of CFSE-positive cells when BM cells derived from WT or CCR1 KO were used. However, when BM cells were derived from CCR5 KO donors, this effect was abolished, with a 13-fold reduction in macrophage recruitment to the liver (Fig. 2D,E). Immunofluorescence staining for bile ducts in liver sections of adoptively transferred mice revealed that recruited CFSE-positive cells specifically surround cholangiocytes (Fig. 2D).

To further study the role of BM-derived macrophages in inflammation and fibrosis in livers of Mdr2-KO mice, 1-month-old Mdr2:CCR5 DKO mice underwent BM transplantation after lethal irradiation with donor BM cells derived from either WT or CCR5<sup>-/-</sup> mice. At the age of 3 months, transplanted mice were sacrificed and liver inflammation and fibrosis was assessed. Accumulation of macrophages (F4-80 staining) and fibrosis (Sirius Red staining) were significantly increased in mice transplanted with WT BM cells, compared to mice receiving BM from CCR5<sup>-/-</sup> mice. These results further support the importance of CCR5 for trafficking and localization of BM-derived macrophages to the damaged liver (Supporting Fig. 2A).

**Ductal and Oval Cell Responses Are Attenuated in Mdr2:CCR5 DKO Mice.** Ductular reaction is thought to have a key role in the initiation and progression of liver cirrhosis. Pan-CK staining for bile ducts in liver sections revealed extensive bile duct proliferation in livers of Mdr2-KO and Mdr2:CCR1 DKO mice, but not in Mdr2:CCR5 DKO livers (Fig. 3A). Mdr2:CCR5 DKO mice also had a 6-fold reduction in positively stained BrdU cells in the portal area, compared to both Mdr2-KO and Mdr2:CCR1 DKO mice (Fig. 3C and Supporting Fig. 2B). Therefore, it is suggested that periductal proliferation correlates with macrophage accumulation, and not liver damage, measured by enzyme levels.

Oval cells, which are liver progenitor cells capable of differentiating into hepatocyte and bile duct epithelial cells, are located in the periductal area and were shown to proliferate around portal veins after liver damage. Gene expression profiling of liver tissue from 3-month-old Mdr2-KO mice suggested that ductular reaction observed in these mice might indeed involve oval cell proliferation. We found that insulin-like growth factor-binding protein (Igfbp)1, secreted phosphoprotein 1 (spp1), CD24, keratin 19 (krt19), and epithelial cell adhesion molecule (EpCAM) that were shown to be expressed in oval cells are all up-regulated

in Mdr2-KO and Mdr2:CCR1 DKO, but not in Mdr2:CCR5 DKO, mice (Fig. 3B)<sup>18-22</sup>. CD24 was recently observed to be expressed on undifferentiated bipotential mouse embryonic liver stem cells and 3,5-diethoxycarbonyl-1,4-dihydrocollidine-induced oval cells<sup>18</sup> as well as a potential marker for a liver cancer stem cell.<sup>23</sup> IHC staining for CD24 indicate that positive cells are involved in the ductular reaction that occurs in the liver injury of Mdr2-KO mice, but are not present in WT mice (Fig. 3B'). The contribution of macrophages to oval cell proliferation and transformation is not yet clear.

**Less Fibrogenesis in Mdr2:CCR5 DKO Mice.** Chronic liver inflammation in humans induces fibrosis that, in time, may progress to cirrhosis. It was recently shown that, in a model of acute liver fibrosis, both CCR1- and CCR5-deficient mice display substantially reduced hepatic fibrosis and macrophage infiltration.<sup>24</sup> In both Mdr2-KO and Mdr2:CCR1 DKO mice, we found severe periductal fibrosis, whereas in Mdr2:CCR5 DKO mice, fibrosis was significantly attenuated. Sirius Red staining revealed that collagen deposits in Mdr2-KO and Mdr2:CCR1 DKO mice were significantly higher than in Mdr2:CCR5 DKO mice (Fig. 3D). Similarly, at the age of 3 months, widespread fibrosis was observed in livers of Mdr2-KO and Mdr2:CCR1 DKO mice, but not in livers of Mdr2:CCR5 DKO mice, which sustained only a minor periductal fibrotic injury. TGF- $\beta$  activates hepatic stellate cells (HSCs), which produce most of the extracellular deposits and matrix metalloproteinases (MMPs) involved in fibrogenesis. We found that mRNA expression of TGF- $\beta$  was significantly higher in livers of Mdr2-KO, compared to Mdr2:CCR5 DKO, mice (Fig. 3E). Furthermore, expression of MMP3 and MMP13 were also reduced significantly in Mdr2:CCR5 DKO mice, compared to Mdr2-KO and Mdr2:CCR1 DKO mice (Supporting Fig. 3A). Expression of  $\alpha$ -SMA, a marker for HSC activation, was also much higher in Mdr2-KO mice, compared to WT, but was not elevated in Mdr2:CCR5 DKO mice (Supporting Fig. 3B). Interestingly, although Mdr2:CCR1 DKO mice developed severe fibrosis, expression of TGF- $\beta$  was reduced in both Mdr2:CCR5 DKO and Mdr2:CCR1 DKO mice.

TGF- $\beta$ 1 induces both epithelial-mesenchymal transition and fibroblast activation and is considered to be a major profibrotic factor. Recently, Igfbp5 has also been shown to induce fibrosis. Furthermore, it also stimulates migration of PBMCs, implicating it in the inflammatory response.<sup>25</sup> Using a gene chip analysis, we found that, in the liver, Igfbp5 is expressed at low

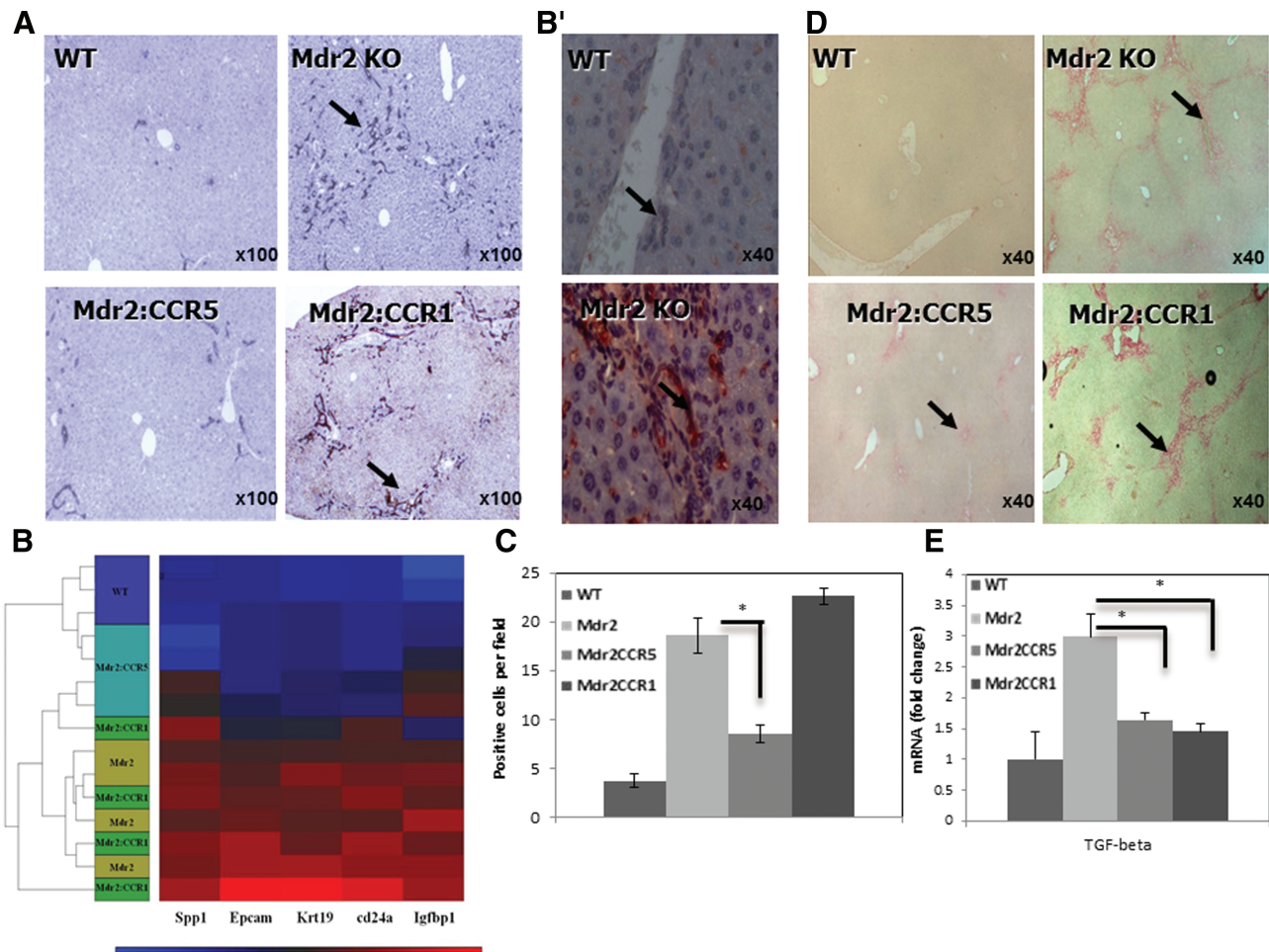


Fig. 3. Reduced inflammation correlates with reduced proliferation and fibrosis in Mdr2:CCR5 DKO mice. (A) Pan-CK IHC staining for cholangiocytes ( $n = 8$ ). (B) Heatmap for genes associated with oval cells. Igfbp1, spp1, CD24, krt19, and EpCAM, which are all up-regulated in Mdr2-KO and Mdr2:CCR1 DKO, but not in Mdr2:CCR5 DKO, mice. (B') IHC staining for cd24-positive cells in Mdr2-KO and WT mice. (C) Assessment of BrdU-positive cells in liver tissue section of different mice strains (\* $P < 0.01$ ). (D) Assessment of extracellular collagen deposits indicated by Sirius Red chemical staining reaction ( $n = 8$ ). (E) Expression of TGF- $\beta$  in liver extracts, as determined by real-time PCR (\* $P < 0.01$ ).

levels. Levels of Igfbp1 and, more dominantly, Igfbp7 are up-regulated in Mdr2-KO mice, down-regulated in Mdr2:CCR5 DKO mice, and up-regulated in livers of Mdr2:CCR1 DKO mice. Levels of Igfbp2, -3, and -4 remain the same (Supporting Fig. 3C). The importance of these genes to liver fibrosis and inflammation is not yet fully understood. However, recent studies have demonstrated that Igfbp7, which is highly expressed in Mdr2:CCR1 DKO mice, functions as a potential tumor suppressor for HCC.<sup>26</sup> This may explain why, in the presence of inflammation and fibrosis, growth of tumors in Mdr2:CCR1 DKO mice is attenuated.

**Less HCC in Mdr2:CCR5 DKO Mice.** Here, we showed that liver fibrosis in Mdr2-KO mice is dependent on CCR5 expression. In humans, fibrosis is believed to be a prerequisite for HCC. To test the effect of

CCR5 and CCR1 depletion on tumor development, we performed monthly MRI scans of Mdr2-KO, Mdr2:CCR1 DKO, and Mdr2:CCR5 DKO mice starting from the age of 9 months. At the age of 9 months, all strains exhibited hepatomegaly, compared to age-matched WT controls. At the age of 16 months, MRI scanning revealed that 75% of Mdr2 KO mice had detectable tumors in the liver, as opposed to only 33% of Mdr2:CCR5 DKO mice (Fig. 4A). Interestingly, tumors in Mdr2:CCR1 DKO mice were already detectable at 13 months of age, and by the age of 16 months 88% had detectable tumors, suggesting that tumorigenesis in these mice is not affected. At the age of 16 months, Mdr2-KO and Mdr2:CCR1 DKO mice revealed severe inflammation associated with fibrosis and increased body/liver index (Fig. 4B). In accord with MRI scanning, macroscopical analysis of harvested

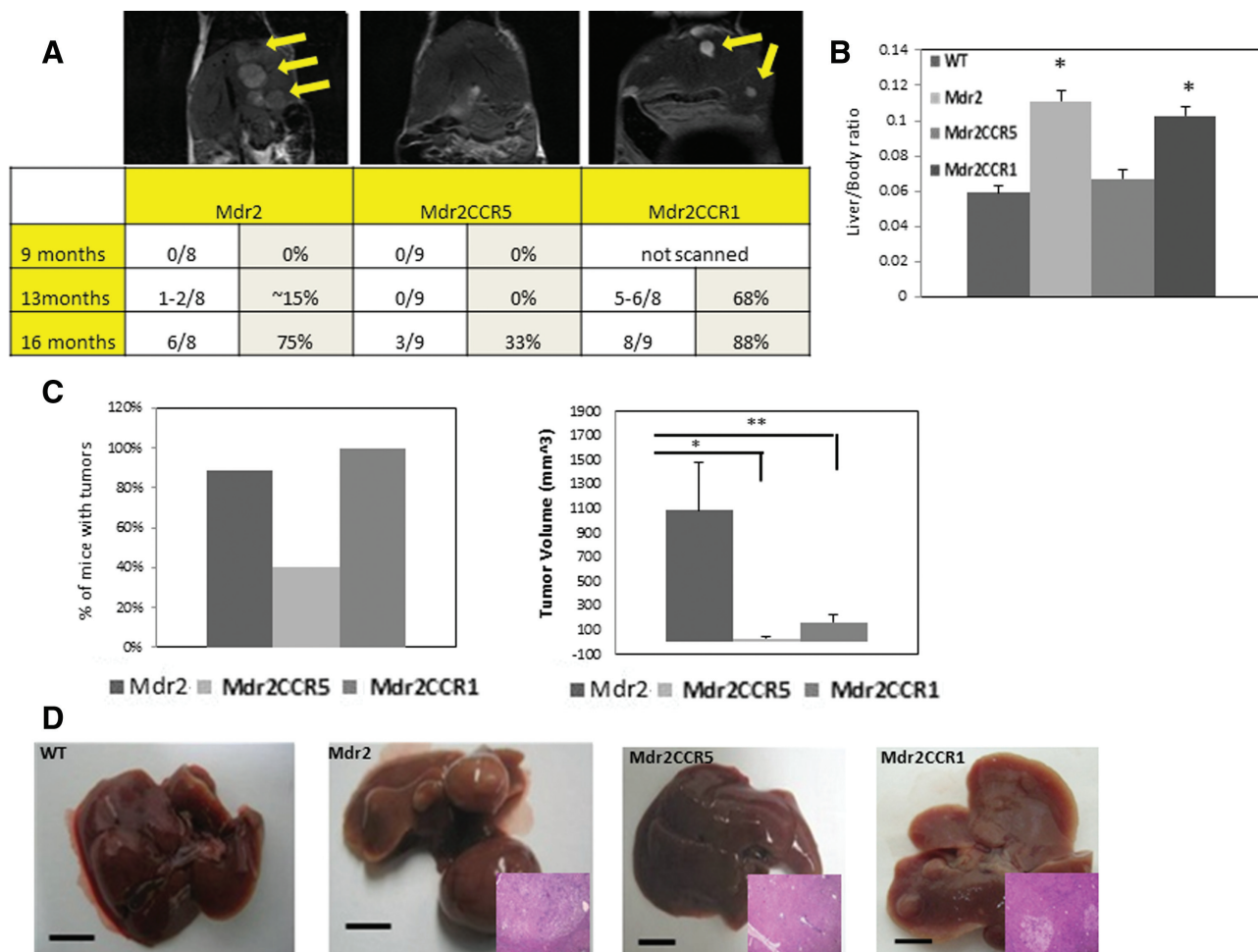


Fig. 4. CCR5 depletion reduces HCC incidence in the Mdr2 KO model. (A) We evaluated tumor formation using MRI scanning of all three groups of mice from the age of 9 months. Visible tumors can be found in Mdr2-KO mice as early as 13 months of age. Representative images of MRI scanning at 16 months of age were chosen for all mouse groups with the number of mice with visible tumors indicated below ( $n = 8-9/\text{group}$ ). (B) Hepatomegaly in mice represented by the ratio of liver/body index. (C) Incidence of HCC in Mdr2-KO, Mdr2:CCR1, and Mdr2:CCR5 DKO mice at the age of 16 months ( $n = 7-12/\text{group}$ ). (D) Tumors were measured and counted in mice 16 months of age. Total tumor volume per mouse was calculated from all tumors larger than 2 mm ( $n = 7-12/\text{group}$ ). (E) Representative images of harvested liver and tumors. Note: pale and rigid appearance of liver in Mdr2-KO and Mdr2:CCR1 mice versus normally colored (red) and perfuse liver of Mdr2:CCR5 DKO mice that looks similar to WT liver. H&E liver sections revealing numerous internal tumors and dysplastic nodules accompanied by ongoing inflammation in Mdr2-KO and Mdr2:CCR1 DKO mice, compared with mild inflammation and normal parenchyma in Mdr2:CCR5 DKO mice. For all experiments: \* $P < 0.01$ ; \*\* $P < 0.05$ .

livers from 16-month-old mice revealed that 90% of Mdr2-KO and 95% of Mdr2:CCR1 DKO mice had notable scattered tumors. Knocking out CCR5 resulted in a 60% reduction in tumor development (Fig. 4C). Furthermore, Mdr2:CCR5 DKO mice that did develop tumors had significantly fewer and smaller tumors, compared to Mdr2 KO mice, resulting in a 20-fold decrease in tumor volume (Fig. 4C). Furthermore, hematoxylin and eosin (H&E) staining of livers from 16-month-old mice revealed that in Mdr2:CCR5 DKO mice that had no macroscopically detected tumors; there was only a mild inflammatory process with a tumor-clear profile and no dysplastic nodules (Fig. 4D).

Remarkably, however, Mdr2:CCR1 DKO mice, which began developing tumors earlier than Mdr2-KO mice, had smaller tumors, with a 5-fold decrease in tumor volume, compared to Mdr2-KO mice (Fig. 4E). This may indicate that whereas CCR1 is not crucial in the initiation of inflammatory damage, it may be critical in tumor progression, possibly by controlling the recruitment of the immune cells that support tumor growth.

## Discussion

Here we show that the chemokine receptor, CCR5, is at the heart of the inflammatory response that

induces tumorigenesis. Macrophages that seem to be the main provokers of the ongoing inflammation in Mdr2-KO mice are completely dependent on CCR5 for their recruitment into the liver. The involvement of macrophages in tumor development and progression is undisputed.<sup>27</sup> Several studies that used the diethylnitrosamine-induced HCC mouse model showed that tumor formation can be induced by targeting distinct pathways, yet all pointed to inflammation as a key player in this process.<sup>28-30</sup> Park et al.'s group reported that steatohepatitis, a common clinical condition, is a significant risk factor for HCC in a mouse model. In this case, the carcinogenic effect was mediated by interleukin (IL)-6 and TNF- $\alpha$ .<sup>29</sup> Furthermore, TNF- $\alpha$  was previously shown to be a significant contributor to inflammation in Mdr2-KO mice.<sup>15</sup> Considering that both TNF- $\alpha$  and IL-6 are secreted by macrophages, it is likely that these findings are very relevant to our results.

The involvement of the CCR5 ligand, RANTES, in cancer has been studied mainly in breast cancer. In this disease, the majority of investigations claim a tumor-promoting role for RANTES.<sup>31</sup> RANTES levels were highly correlated with advanced and progressed disease in breast cancer, and suggested that the chemokine is directly involved in disease course. This hypothesis was proven correct in several studies that have manipulated the activities or expression of RANTES in animal model systems of breast cancer in mice. Different approaches—including the use of small interfering RNA to RANTES, the CCR5 antagonist, met-RANTES, and maraviroc, expression of the  $\Delta 32$  CCR5, and overexpression of RANTES—have demonstrated that RANTES promotes tumor growth and disease progression.<sup>32-35</sup>

Our results not only bolster the evidence that macrophages are indeed critical in inflammation-induced tumorigenesis, but also suggest that CCR5/RANTES axis is pivotal in their recruitment to the liver. It is conceivable that CCR5 is involved in several pathways of tumor development, including in both the inflammatory response that induces oncogenic stress and the recruitment of cells that facilitates tumor progression and maintenance. Consequently, antagonists for CCR5 and CCR1, currently in clinical development, may prove useful in the prevention and treatment of liver inflammation, fibrosis, and HCC.

## References

- Balkwill F, Mantovani A. Inflammation and cancer: back to Virchow? *Lancet* 2001;357:539-545.
- Clevers H. At the crossroads of inflammation and cancer. *Cell* 2004;118:671-674.
- Karin M, Lawrence T, Nizet V. Innate immunity gone awry: linking microbial infections to chronic inflammation and cancer. *Cell* 2006;124:823-835.
- Bruix J, Boix L, Sala M, Llovet JM. Focus on hepatocellular carcinoma. *Cancer Cell* 2004;5:215-219.
- Llovet JM, Burroughs A, Bruix J. Hepatocellular carcinoma. *Lancet* 2003;362:1907-1917.
- Nakamoto Y, Guidotti LG, Kuhlen CV, Fowler P, Chisari FV. Immune pathogenesis of hepatocellular carcinoma. *J Exp Med* 1998;188:341-350.
- Block TM, Mehta AS, Fimmel CJ, Jordan R. Molecular viral oncology of hepatocellular carcinoma. *Oncogene* 2003;22:5093-5107.
- Vicari AP, Caux C. Chemokines in cancer. *Cytokine Growth Factor Rev* 2002;13:143-154.
- Balkwill F. Cancer and the chemokine network. *Nat Rev Cancer* 2004;4:540-550.
- Pakianathan DR, Kuta EG, Artis DR, Skelton NJ, Hebert CA. Distinct but overlapping epitopes for the interaction of a CC-chemokine with CCR1, CCR3, and CCR5. *Biochemistry* 1997;36:9642-9648.
- Sozzani S, Luini W, Borsatti A, Polentarutti N, Zhou D, Piemonti L, et al. Receptor expression and responsiveness of human dendritic cells to a defined set of CC and CXC chemokines. *J Immunol* 1997;159:1993-2000.
- Weiss ID, Shoham H, Wald O, Wald H, Beider K, Abraham M, et al. Ccr5 deficiency regulates the proliferation and trafficking of natural killer cells under physiological conditions. *Cytokine* 2011;54:249-257.
- Mauad TH, van Nieuwkerk CM, Dingemans KP, Smit JJ, Schinkel AH, Notenboom RG, et al. Mice with homozygous disruption of the mdr2 P-glycoprotein gene. A novel animal model for studies of non-suppurative cholangitis and hepatocarcinogenesis. *Am J Pathol* 1994;145:1237-1245.
- Popov Y, Patsenker E, Fickert P, Trauner M, Schuppan D. Mdr2 (Abcb4)-/- mice spontaneously develop severe biliary fibrosis via massive dysregulation of pro- and antifibrogenic genes. *J Hepatol* 2005;43:1045-1054.
- Pikarsky E, Porat RM, Stein I, Abramovitch R, Amit S, Kasem S, et al. NF- $\kappa$ B functions as a tumour promoter in inflammation-associated cancer. *Nature* 2004;431:461-466.
- Katzenellenbogen M, Mizrahi L, Pappo O, Klopstock N, Olam D, Barash H, et al. Molecular mechanisms of the chemopreventive effect on hepatocellular carcinoma development in Mdr2 knockout mice. *Mol Cancer Ther* 2007;6:1283-1291.
- Wald O, Pappo O, Ari ZB, Azzaria E, Wiess ID, Gafnovitch I, et al. The CCR5Delta32 allele is associated with reduced liver inflammation in hepatitis C virus infection. *Eur J Immunogenet* 2004;31:249-252.
- Qiu Q, Hernandez JC, Dean AM, Rao PH, Darlington GJ. CD24-positive cells from normal adult mouse liver are hepatocyte progenitor cells. *Stem Cells Dev* 2011;20:2177-2188.
- Okabe M, Tsukahara Y, Tanaka M, Suzuki K, Saito S, Kamiya Y, et al. Potential hepatic stem cells reside in EpCAM+ cells of normal and injured mouse liver. *Development* 2009;136:1951-1960.
- Batusic DS, Cimica V, Chen Y, Tron K, Hollemann T, Pieler T, Rama-dori G. Identification of genes specific to "oval cells" in the rat 2-acetylaminofluorene/partial hepatectomy model. *Histochem Cell Biol* 2005;124:245-260.
- Tirnitz-Parker JE, Tonkin JN, Knight B, Olynyk JK, Yeoh GC. Isolation, culture, and immortalisation of hepatic oval cells from adult mice fed a choline-deficient, ethionine-supplemented diet. *Int J Biochem Cell Biol* 2007;39:2226-2239.
- Xu J, Deng X, Demetriou AA, Farkas DL, Hui T, Wang C. Factors released from cholestatic rat livers possibly involved in inducing bone marrow hepatic stem cell priming. *Stem Cells Dev* 2008;17:143-155.
- Lee TK, Castilho A, Cheung VC, Tang KH, Ma S, Ng IO. CD24(+) liver tumor-initiating cells drive self-renewal and tumor initiation

- through STAT3-mediated NANOG regulation. *Cell Stem Cell* 2011;9:50-63.
- 24. Seki E, De Minicis S, Gwak GY, Kluwe J, Inokuchi S, Bursill CA, et al. CCR1 and CCR5 promote hepatic fibrosis in mice. *J Clin Invest* 2009;119:1858-1870.
  - 25. Sureshbabu A, Okajima H, Yamanaka D, Shastri S, Tonner E, Rae C, et al. IGFBP-5 induces epithelial and fibroblast responses consistent with the fibrotic response. *Biochem Soc Trans* 2009;37:882-885.
  - 26. Chen D, Siddiq A, Emdad L, Rajasekaran D, Gredler R, Shen XN, et al. Insulin-like growth factor-binding protein-7 (IGFBP7): a promising gene therapeutic for hepatocellular carcinoma (HCC). *Mol Ther* 2013 Jan 15. doi:10.1038/mt.2012.282.
  - 27. Grivennikov SI, Greten FR, Karin M. Immunity, inflammation, and cancer. *Cell* 2010;140:883-899.
  - 28. Szabo G, Wands JR, Eken A, Osnas NA, Weinman SA, Machida K, Joe Wang H. Alcohol and hepatitis C virus—interactions in immune dysfunctions and liver damage. *Alcohol Clin Exp Res* 2010;34:1675-1686.
  - 29. Park EJ, Lee JH, Yu GY, He G, Ali SR, Holzer RG, et al. Dietary and genetic obesity promote liver inflammation and tumorigenesis by enhancing IL-6 and TNF expression. *Cell* 2010;140:197-208.
  - 30. Maeda S, Kamata H, Luo JL, Leffert H, Karin M. IKKbeta couples hepatocyte death to cytokine-driven compensatory proliferation that promotes chemical hepatocarcinogenesis. *Cell* 2005;121:977-990.
  - 31. Soria G, Ofri-Shahak M, Haas I, Yaal-Hahoshen N, Leider-Trejo L, Leibovich-Rivkin T, et al. Inflammatory mediators in breast cancer: coordinated expression of TNFalpha & IL-1beta with CCL2 & CCL5 and effects on epithelial-to-mesenchymal transition. *BMC Cancer* 2011;11:130.
  - 32. Karnoub AE, Dash AB, Vo AP, Sullivan A, Brooks MW, Bell GW, et al. Mesenchymal stem cells within tumour stroma promote breast cancer metastasis. *Nature* 2007;449:557-563.
  - 33. Robinson SC, Scott KA, Wilson JL, Thompson RG, Proudfoot AE, Balkwill FR. A chemokine receptor antagonist inhibits experimental breast tumor growth. *Cancer Res* 2003;63:8360-8365.
  - 34. Stormes KA, Lemken CA, Lepre JV, Marinucci MN, Kurt RA. Inhibition of metastasis by inhibition of tumor-derived CCL5. *Breast Cancer Res Treat* 2005;89:209-212.
  - 35. Velasco-Velazquez M, Jiao X, De La Fuente M, Pestell TG, Ertel A, Lisanti MP, Pestell RG. CCR5 antagonist blocks metastasis of basal breast cancer cells. *Cancer Res* 2012;72:3839-3850.